QUANTIFYING THE IMPACT OF TEMPORAL ANALYSIS OF PRODUCTS REACTOR INITIAL STATE UNCERTAINTIES ON KINETIC PARAMETERS

A PREPRINT

Adam Yonge
College of Engineering
Georgia Institute of Technology
Atlanta, GA 30332
ayonge3@gatech.edu

M. Ross Kunz
Department of Biological and Chemical Processing
Idaho National Laboratory
Idaho Falls, ID 83415
ross.kunz@inl.gov

Gabriel Gusmão
College of Engineering
Georgia Institute of Technology
Atlanta, GA 30332
gusmaogabriels@gatech.edu

Zongtang Fang
Department of Biological and Chemical Processing
Idaho National Laboratory
Idaho Falls, ID 83415
zongtang.fang@inl.gov

Rakesh Batchu
Department of Biological and Chemical Processing
Idaho National Laboratory
Idaho Falls, ID 83415
rakesh.batchu@inl.gov

Rebecca Fushimi
Department of Biological and Chemical Processing
Idaho National Laboratory
Idaho Falls, ID 83415
rebecca.fushimi@inl.gov

Andrew J. Medford
College of Engineering
Georgia Institute of Technology
Atlanta, GA 30332
ajm@gatech.edu

September 20, 2021

ABSTRACT

The temporal analysis of products (TAP) reactor provides a route to extract intrinsic kinetics from transient measurements. Current TAP uncertainty quantification only considers the experimental noise present in the outlet flow signal. Additional sources of uncertainty such as initial surface coverages, catalyst zone location, inert void fraction, gas pulse intensity and pulse delay, are not included. For this reason, a framework for quantifying initial state uncertainties present in TAP experiments is presented and applied to a carbon monoxide oxidation case study. Two methods for quantifying these sources of uncertainty are introduced. The first utilizes initial state sensitivities to approximate the parameter variances and provide insights into the structural certainty of the model. The second generates parameter confidence distributions through an ensemble-based sampling algorithm. The initial state covariance matrix can ultimately be merged with the experimental noise covariance matrix, providing a unified description of the parameter uncertainties for a TAP experiment.

***K*eywords** Transient kinetics · Uncertainty Quantification · Micro-kinetic Modeling · Inverse Problems

1 Introduction

The scale-up of chemical processes often hinges on the design of catalytic materials through kinetic modeling [1]. However, obtaining flexibility (i.e. accurately predicting reaction rates and selectivities under diverse operating conditions) [2] is a challenge for microkinetic model construction. Many experimental and computational methods exist for constructing reliable models, but each can struggle with efficiency and information density [3]. For example, the error associated with adsorption energies and reaction barriers extracted from surface science experiments or density functional theory (DFT) calculations is generally accepted to be on the order of 20 kJ/mol [4, 2, 5]. Transient experiments, which can rapidly generate large volumes of data and identify potential reaction intermediates of elementary steps are an underutilized alternative to these traditional approaches, but they require extensive postprocessing of experimental data. The TAP reactor system is particularly valuable, in structure-activity relationships as it captures catalyst state changes in milli-second time resolution over a series of reactant pulses [6, 7, 8]. However, the error associated with kinetic parameters extracted from TAP experiments has not been extensively studied.

The quantification of model parameter and reaction/reactor simulation uncertainties has become more common in the last decade [2, 9, 10]. For example, the uncertainties of DFT calculations have been determined and propagated to steady-state simulations, providing useful insights into the distributions and mechanistic overlaps between the turnover frequencies of experimentally observed products [11]. Elsewhere, automated methods of reducing uncertainty in kinetic parameters have been implemented [12, 13]. Vlachos et al. have performed extensive research on the topic [14, 15, 16, 17] and recently published several broadly applicable programs and direct applications to ethane dehydrogenation [18, 19]. Moreover, Savara and Walker recently released the CheKiPEUQ code for Bayesian parameter estimation of kinetic models based on experiment and theory [20]. Generally, uncertainty quantification (UQ) allows investigators to draw stronger conclusions than purely deterministic analyses since confidence intervals can be placed around quantities of interest (QoI).

Though some investigations have been performed, TAP UQ has been studied to a lesser extent. Exceptions include Yablonsky et al. discussing the influence of uncertainties on the results of TAP based chemical-calculus [21, 22], as well as the TAPsolver Python program that constructs covariance matrices for PDE-constrained optimized parameters [23]. The complexity of the noise present in the outlet flow signal has also been explored [24, 25], but there are lingering uncertainties present. In particular, when performing PDE-constrained optimization, all initial states must be defined (e.g. pulse intensity, pulse delay, reactor temperature, surface composition) before a simulation can be performed, as illustrated in Figure 1. The values of these initial states are assumed to be known exactly, but often contain their own level of uncertainty which in turn leads to uncertainties in the simulated outlet fluxes and associated fitted kinetic parameters.

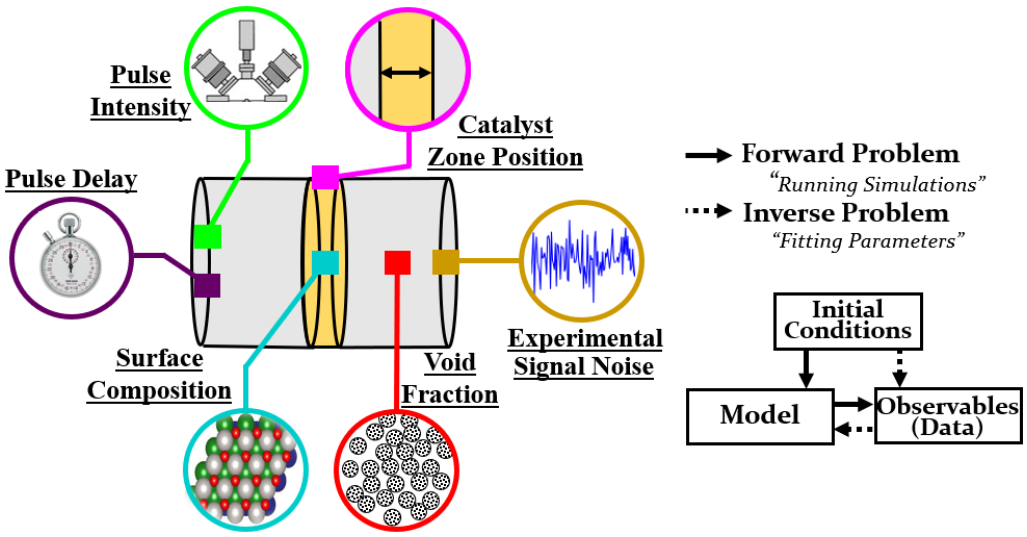

Figure 1: Various sources of uncertainty present in the TAP reactor setup and experimental data, which have an undetermined impact on the kinetic information extracted while modeling. The forward and inverse formulation of TAP experiments can provide researchers with this information.

Presently, there is no standard approach for analyzing the uncertainty resulting from initial states of PDE-constrained optimization of kinetic parameters from TAP experiments. For this reason, the impact of the uncertainties of the pulse intensity, pulse delay, catalyst zone position, void fraction and surface composition on fitted parameters are studied. The methods developed for gaining qualitative and quantitative insights from these sources are presented in Figure 2. The sensitivity-based algorithm is computationally efficient and provides a rough estimate of parameter variance and structural certainty. The ensemble-based sampling algorithm is more computationally expensive but yields a more detailed covariance matrix for quantitative associations. A carbon monoxide oxidation experimental data set is used as a case study, where the mechanism, set of kinetic parameters, and their associated uncertainties have previously been explored [23]. Comparisons between the impact of uncertainty in the initial state and the experimental noise are made. The results indicate that when the objective function is used to identify reasonable ranges of initial states, the resulting uncertainty is larger than the experimental uncertainty, while both are significantly lower than typical uncertainty from computational chemistry.

2 Methodology

2.1 Problem definition and numerical tools

PDEs are often used to interpret the complex transport and reactions occurring during TAP experiments [6]. Knudsen diffusion is the dominant driving force of transport, while a series of gas-surface and surface-surface reactions can take place in the catalyst zone at the center of the reactor [26]. Details of the PDEs have been thoroughly outlined elsewhere [6]. TAPsolver, a Python package for the processing of TAP experimental data, is used to perform the analysis presented here [23]. This methodology can be framed as the forward and inverse problem (outlined in Figure 1). The

forward problem is analyzed when the initial stat es and models are known and the observables (or outlet data) are to be determined. The inverse problem involves the observables being specified, while the information related to the model is unknown. This is the primary terminology used to discuss the newly developed methods. A carbon monoxide oxidation case study is used to analyze the sources of uncertainty in the TAP inverse problem and the TAPsolver package is used for all forward and inverse simulations. The case study consists of co-pulsing of carbon monoxide and oxygen over a partially oxidized platinum catalyst. The mechanism used to fit the experimental data is

$$CO + * \underset{k_1^b}{\overset{k_1^f}{\rightleftharpoons}} CO^* \tag{1}$$

$$O_2 + * \underset{k_2^b}{\overset{k_2^f}{\rightleftharpoons}} O_2^* \tag{2}$$

$$O_2^* + * \xrightarrow{k_3^f} 2O^* \tag{3}$$

$$CO + O^* \xrightarrow{k_4^f} CO_2 + * \tag{4}$$

The kinetic parameters fitted to the experimental data were found and are presented in Table 1. Minor variations between the values in Table 1 and the prior analysis are due to the more accurate specification of the initial conditions in this analysis [23]. The reactor configuration is provided in the supplementary information (Section 1). These details include pulse intensities and times, surface compositions, zone lengths and void fractions (i.e. all initial conditions), and values of the kinetic parameters.

Table 1: Kinetic parameters determined through the analysis of carbon monoxide oxidation experimental data over a platinum catalyst [23].

Reaction	Value	Standard Deviation	IQR	Units
k_1^f	$2.80 * 10^1$	$2.79 * 10^{-1}$	$3.77 * 10^{-1}$	$\frac{cm^3}{nmols}$
k_1^b	$1.06 * 10^1$	$1.02 * 10^{-1}$	$1.38 * 10^{-1}$	$\frac{1}{s}$
k_2^f	$9.63 * 10^{-1}$	$6.69 * 10^{-3}$	$9.03 * 10^{-3}$	$\frac{cm^3}{nmols}$
k_2^b	$6.56 * 10^0$	$7.48 * 10^{-2}$	$1.01 * 10^{-1}$	$\frac{1}{s}$
k_3^f	$9.05 * 10^{-3}$	$1.41 * 10^{-4}$	$1.90 * 10^{-4}$	$\frac{cm^3}{nmols}$
k_4^f	$4.45 * 10^0$	$2.54 * 10^{-2}$	$3.43 * 10^{-2}$	$\frac{cm^3}{nmols}$

One source of uncertainty is the noise present in the experimental data from the mass spectrometer signal, and this experimental noise translates to uncertainty in the fitted kinetic parameters. Unlike other sources of uncertainty, experimental noise is present in the objective function (i.e. parameter optimization involves the presence of noise in the signal). The objective function is defined as

$$J^N = \sum_{i=0}^{G} \sum_{j=0}^{T} \frac{(F_{syn} - F_{obs})_{i,j}^2}{2\hat{\sigma}_{i,j}^2} \tag{5}$$

where J^N is the objective function scaled to the experimental standard deviation, $\hat{\sigma}_{i,j}$ (determined via multiple measurements or analysis of baseline signal). At the minima of the objective function, the curvature is positive-definite and approximately quadratic. This shape allows confidence intervals to be constructed through the analysis of the Hessian matrix. The Hessian is determined by calculating the second-order derivatives in the objective space, written as

$$H_{J^N}(k) = \frac{\partial^2 J^N}{\partial k^2} \tag{6}$$

where k is the set of kinetic parameters in the model. The covariance and confidence intervals are then estimated through

$$P_N \approx H_J(k)^{-1} \tag{7}$$

and subsequently taking the square-root of the diagonal values

$$\sigma_i \approx \sqrt{P_{i,i}} \tag{8}$$

where P_N is the covariance matrix and σ_i is the standard deviation of parameter i due to experimental signal noise. The inter-quartile range (IQR) can also be computed as $IQR_i = 1.35\sigma_i$ assuming the distribution is normal, and is useful for comparing uncertainties with distributions that are not Gaussian. The uncertainty due to experimental noise was calculated and is provided in Table 1.

2.2 Initial State Uncertainty

When the forward and inverse methodology are applied to TAP experiments, it is often assumed that the initial conditions are known exactly. Unfortunately, this is rarely the case and these conditions have some degree of uncertainty associated with them. Directly connecting these uncertainties to the simulated outlet flux in an analytical manner is not possible and variations of these initial conditions must be made numerically. We utilize two approaches for numerical analysis of initial state uncertainty: sensitivity analysis and ensemble sampling. These approaches are shown schematically in Fig. 2 and described below.

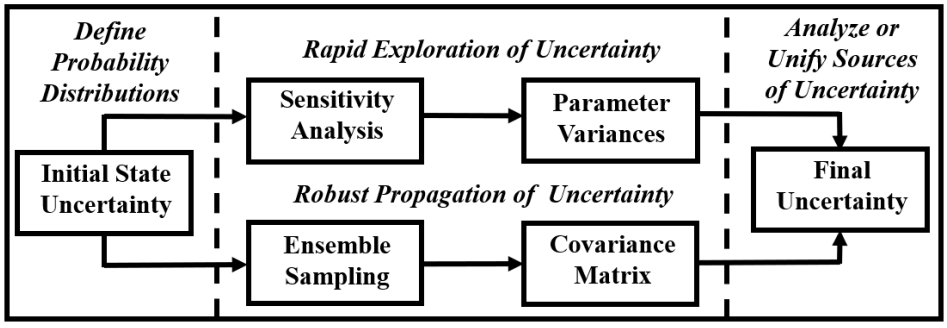

Figure 2: The sensitivity and ensemble approaches offer two ways to quantify the impact initial state uncertainties have on the uncertainty of kinetic parameters. The sensitivity approach is computationally inexpensive but relies on more assumptions, while the ensemble-sampling approach is more computationally expensive and relies on fewer assumptions.

2.2.1 Sensitivity-based analysis

A sensitivity-based approach can be useful for identifying initial conditions that significantly shift parameter values at a low computational cost. The methodology consists of selecting a parameter and defining a range of relevant values for exploration. Defining relevant conditions can vary depending on the context, but can generally be understood as physically meaningful (e.g. void fractions or surface coverages between zero and one) or within experimentally possible values. From there, several different points or a uniform distribution within the domain can be generated and the optimization routine (minimizing Equation 5) applied to each condition. The results reveal both the influence of initial conditions on the parameters, as well as their influence on the objective function, providing *quantitative* insight into the values of the initial conditions that are most consistent with the experimental measurements. In addition, the results can provide *qualitative* insight into the structural (e.g. mechanistic model) uncertainty, where discontinuities in the observed parameters indicate a change in the structure of the elementary reactions that are most consistent with the experimental data. Similarly, the variance of parameters can be approximated from the sensitivity analysis approach [27]. The local sensitivity (S) can be approximated as

$$S_{i,I} = \frac{\partial k}{\partial I} \approx \frac{\Delta k}{\Delta I} \tag{9}$$

where k is the kinetic parameter of interest, I is the initial condition of interest, while Δk and ΔI are small increments used for a finite difference approximation of the derivative. The variance of the kinetic parameter (σ_i) is then calculated by multiplying the local sensitivity with an assumed initial state standard deviation ($\tilde{\sigma}_I$), written as

$$\sigma_{i,I} = S_{i,I}\tilde{\sigma}_I \tag{10}$$

Equation 10 can be expanded to approximate the kinetic parameter variance involving all desired initial conditions (N) in the form

$$\bar{\sigma_i} = \sqrt{\sum_{I=0} S_{i,I}^2 \tilde{\sigma}_I^2} \tag{11}$$

where $\bar{\sigma_i}$ is the total standard deviation on parameter i due to all initial conditions.

2.2.2 Ensemble-based analysis

The sensitivity-based approach only provides an approximation of the variance based on the assumption that the objective function responds linearly to the parameter, and provides no information about co-variances. A more detailed, but more computationally expensive alternative is the ensemble-based approach. To use the ensemble-based approach, a probability distribution must be defined over each of the initial states. This distribution can then be used to generate random samples that are used to create an ensemble of inverse models. In this study, we assume that initial conditions that are effectively unbounded (e.g. pulse intensities and void fraction) are described by a normal distribution (see Supplementary Information (Section 2), and initial conditions that are bounded on $[0, 1]$ (e.g. surface coverages) are

described by the beta distribution [28]. The normal distribution is defined as

$$f(x) = \frac{1}{\tilde{\sigma}_I \sqrt{(2\pi)}} \exp\left(-\frac{1}{2}\left(\frac{x-\mu_I}{\tilde{\sigma}_I}\right)^2\right) \tag{12}$$

where μ_I is the mean and $\tilde{\sigma}_I$ is the standard deviation associated with the uncertainty for the initial state I. The beta distribution is defined as

$$f(x) = \frac{1}{B(\alpha,\beta)} x^{\alpha-1}(1-x)^{\beta-1} \tag{13}$$

where α and β represent the shape parameters of the distribution and B is a normalization factor given by

$$B(\alpha,\beta) = \int_0^1 t^{\alpha-1}(1-t)^{\beta-1} dt. \tag{14}$$

The resulting parameter ensembles can be used to compute a parameter covariance matrix

$$P_I = cov\left(M_{s,k}\right) \tag{15}$$

where $M_{s,k}$ is the matrix consisting of the refitted kinetic parameters (k) for each member of the ensemble (s). Assuming no correlation between the covariance of the initial state and experimental noise, the two can be added as

$$P_T = P_I + P_N \tag{16}$$

where P_T is the covariance matrix that includes uncertainty from the experimental signal and the initial states. Any sampling algorithm can be used to perform this analysis, but the random sampling algorithm in Scipy was used to collect and propagate the uncertainty from all distributions in this study [29, 30]. We also note that while the ensemble approach is computationally expensive, it is also "proudly parallel", since each member of the ensemble can be run independently, enabling relatively rapid estimates if many cores are available.

3 Results

3.1 Sensitivity Analysis and Continuous Parameter Variation

There are a total of 8 initial conditions being considered in the carbon monoxide oxidation case study, with 6 kinetic parameters included in the mechanism, resulting in a total of 48 sensitivities. For brevity, we only show the sensitivity of parameter k_1^f, or the adsorption of carbon monoxide, in Figure 3. The remaining figures are qualitatively similar, and are provided in the supplementary information (Sections 3 - 10). Alongside the variation in the value of the kinetic parameter (black circles), the objective function value is also shown (red squares) to provide insight into the initial conditions that are most consistent with the experimental observations.

The first initial conditions varied are the surface coverages of the platinum catalyst. The assumed initial coverage of carbon monoxide and molecular oxygen are 0.0, while atomic oxygen is assumed to be 0.5. The range under which each species coverage was varied was not identical, with the species having an assumed initial coverage of 0 (i.e. CO^* and O_2^*) only changing between 0 and 0.2 and atomic oxygen coverage between 0 and 1. This was due to the divergence of the objective function at more extreme values for the low coverage species. In the case of O* coverage, the value of k_1^f increases exponentially near the boundaries of 0 and 1. Simultaneously, there is a significant increase in the value of the objective function, indicating that the model is no longer able to accurately describe the experimental data. This makes intuitive sense, since a complete coverage of atomic oxygen or open sites will lead to either no adsorption of carbon monoxide or no oxygen available for conversion to carbon dioxide. A similar observation can be made in the molecular oxygen figure, where a discontinuous change occurs in the value of k_1^f and the objective function near a coverage of 0.02. When the molecular oxygen coverage reaches this value, the elementary reactions for molecular oxygen adsorption and desorption no longer adequately capture the experimental observations (resulting in a discontinuous increase in the objective function). The objective function does not experience a discontinuity as a function of carbon monoxide coverage, but does increase monotonically as the coverage is increased.

The next set of initial conditions explored are the pulse intensities and delays. The initial pulse intensities for both carbon monoxide and molecular oxygen are 5 nmols and the delay in carbon monoxide pulsing was 10 ms. The intensities were varied between 3 and 8 nmols, while the delay was adjusted between 0 and 40 ms. Near the experimentally assumed carbon monoxide pulse intensity, there is only a limited change in the value of the adsorption parameter. However, when the intensity is reduced below 4 nmol, the parameter value increases by orders of magnitude and the objective function also increases sharply, indicating that the values are inconsistent with the experimental data. A unique change in the molecular oxygen intensity variation is also present, where oxygen intensities below approximately 4.1 nmols results in no change to the kinetic parameter, while the parameter varies linearly at higher values. At lower intensities, the objective function also increases sharply, indicating that these values are not consistent with the experimental data. Varying the pulse delay caused less dramatic changes to parameter values. The carbon monoxide delay resulted in a linear decrease in the adsorption parameter, along with a decrease in the objective function value. This suggests that a longer CO pulse delay is slightly more consistent with the experiment, which could be due to an unknown delay in the experiment, or an artifact of an imperfect description of diffusion. However, the decreases in the kinetic parameter and objective function are limited, suggesting that the effect can be neglected.

The remaining two initial conditions explored are the catalyst zone location and the inert zone void fraction. The experimentally assumed values for each are 2.89 cm (i.e. the center of the reactor) and 0.4, respectively. Although the range of location values explored results in a substantial variation (a factor of $\sim$2) in the parameter, the trend is generally linear. The void fraction values vary more significantly with an exponential change in the kinetic parameter at low void fractions. When the reactor is assumed to have an inert material with a void fraction of 0, the kinetic parameters increase and follow an inconsistent, chaotic trend, and the objective function increases sharply. This indicates that assuming the reactor model has a small void fraction (less than 0.25) would be inconsistent with the experimental data.

However, there is a region in the void fraction between 0.2 - 0.4 where the objective function is nearly constant, while the rate constant varies exponentially. This suggests that it is critical to establish a highly accurate void fraction with experimental techniques to reduce the uncertainty in kinetic parameters.

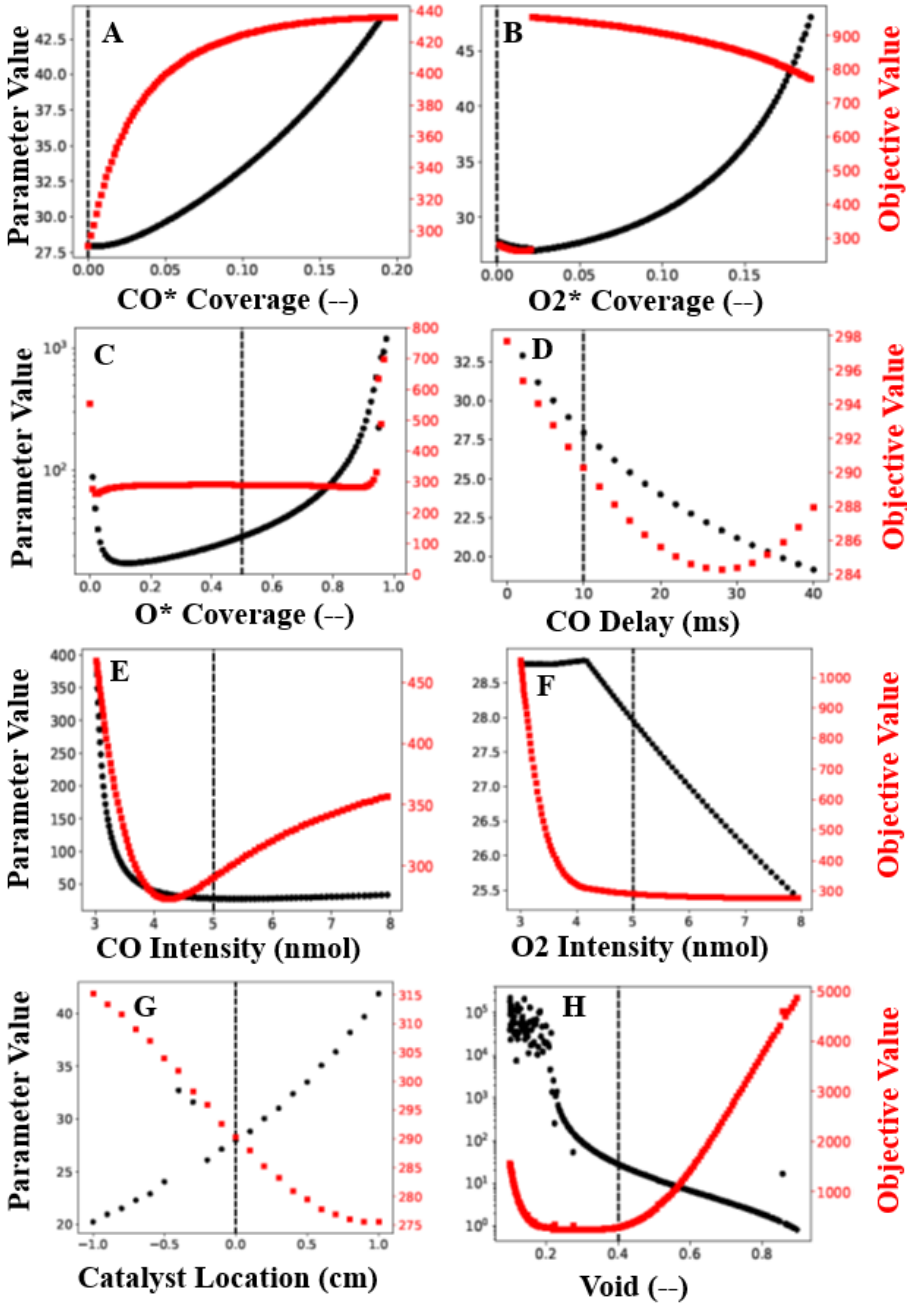

Figure 3: The sensitivity of the kinetic parameter (black dots) and changes in the objective function (red squares) for carbon monoxide adsorption with variations to the surface coverages (a-c), carbon monoxide delay (d), pulse intensities (e-f), catalyst zone location (g), and void fraction (h).

The information related to variations near the experimentally assumed initial conditions for each of the five remaining kinetic parameters are provided in Table 2. This table provides the normalized sensitivity values, where a small step

was made in the initial condition and the value of the parameter was observed. Equation 9 was used to generate the sensitivity values, and the sensitivities were normalized by dividing by the assumed kinetic parameters (i.e. the values found with deterministic initial conditions). The step size for each initial condition is provided in the Δ column. The other columns in the table represent the parameter change being monitored (∂k), while the rows represent the initial condition being varied ($\partial initial$). Full sensitivity plots for each parameter as a function of each initial state are provided in the supplementary information.

Of the initial conditions impacting the adsorption of carbon monoxide (k_1^f), the void fraction has the highest sensitivity (approximately 70). Considering the previous discussion of Figure 3, this was an expected result. The impact the void has on the other parameters explored is less pronounced than for k_1^f, with the exception of k_2^f and k_2^b. A major difference between the impact the void fraction has on k_1^f and $k_2^{f/b}$ is the sensitivity of $k_2^{f/b}$ to other initial conditions. The sensitivity of both $k_2^{f/b}$ to the molecular oxygen coverage is larger than the sensitivity to the void fraction. The molecular oxygen coverage also has the highest impact on the parameter k_3^f by over an order of magnitude, with the void fraction being the second most important. Carbon monoxide coverage was found to be the most impactful initial condition on the value of k_1^b, with the void fraction again being the second most important. Of the initial conditions considered, the pulse delays were consistently found to have the lowest sensitivity. The results indicate that many different initial conditions can have an impact on the values of kinetic parameters.

Sensitivities are useful because they require no assumptions about the uncertainty of the initial conditions. However, as Eq. 10 reveals, the uncertainty of a kinetic parameter is related to both the sensitivity and the uncertainty of the initial conditions. The approximations of the individual kinetic parameter standard deviations for each initial state, calculated using Equation 10, are given in Table 3. The standard deviation of each initial condition is also included in the table, and is consistent with the ensembles used in later sections. Comparing Tables 2 and 3 reveals that differences in uncertainty on each initial state can shift their relative importance. For example, in the case of carbon monoxide adsorption (k_1^f), the O* coverage has a larger impact on the parameter than the void fraction after accounting for initial state uncertainty. The parameter is very sensitive to the void fraction, but since the void fraction is experimentally well determined [28], it has less of an impact on the parameter. This indicates that even approximate estimates of initial state uncertainties are necessary to identify the relative impact between different states on each parameter.

Table 2: Normalized values of the kinetic parameter sensitivities relative to changes in the initial conditions. These values were found through Equation 9 and were normalized by their baseline value (i.e. $(\partial k_i/\partial I)/k_i$). Continuous variations of the initial conditions (like those in Figure 3) can be found in the supplementary information (Sections 3 to 10).

Variable	∂k_1^f	∂k_1^b	∂k_2^f	∂k_2^b	∂k_3^f	∂k_4^b	Step Size (Δ)
∂CO^*	$1.15\cdot 10^{-2}$	$1.76\cdot 10^{1}$	$6.76\cdot 10^{-1}$	$6.82\cdot 10^{-1}$	$3.89\cdot 10^{-2}$	$1.14\cdot 10^{0}$	$3.33\cdot 10^{-3}$ $(-)$
∂O_2^*	$8.62\cdot 10^{-1}$	$2.07\cdot 10^{0}$	$3.94\cdot 10^{1}$	$1.52\cdot 10^{1}$	$4.38\cdot 10^{1}$	$8.47\cdot 10^{-1}$	$3.33\cdot 10^{-3}$ $(-)$
∂O^*	$8.31\cdot 10^{-1}$	$7.26\cdot 10^{-3}$	$1.06\cdot 10^{0}$	$4.93\cdot 10^{-1}$	$1.03\cdot 10^{0}$	$1.02\cdot 10^{0}$	$1.67\cdot 10^{-2}$ $(-)$
∂T^{CO}	$1.31\cdot 10^{-2}$	$1.36\cdot 10^{-2}$	$5.73\cdot 10^{-4}$	$4.32\cdot 10^{-4}$	$3.89\cdot 10^{-4}$	$1.40\cdot 10^{-3}$	$1.00\cdot 10^{0}$ (ms)
$\partial void$	$6.86\cdot 10^{0}$	$3.99\cdot 10^{0}$	$1.53\cdot 10^{1}$	$1.41\cdot 10^{1}$	$8.08\cdot 10^{-1}$	$1.03\cdot 10^{0}$	$5.04\cdot 10^{-3}$ $(-)$

∂loc	$2.41 \cdot 10^{0}$	$7.55 \cdot 10^{-1}$	$8.93 \cdot 10^{-1}$	$4.69 \cdot 10^{0}$	$6.67 \cdot 10^{-2}$	$1.89 \cdot 10^{0}$	$1.00 \cdot 10^{-1}$ (cm)
∂I^{CO}	$6.53 \cdot 10^{-2}$	$4.00 \cdot 10^{-1}$	$2.47 \cdot 10^{-3}$	$6.23 \cdot 10^{-3}$	$1.22 \cdot 10^{-2}$	$3.56 \cdot 10^{-2}$	$1.60 \cdot 10^{-2}$ $(nmol)$
∂I^{O_2}	$2.80 \cdot 10^{-2}$	$4.72 \cdot 10^{-2}$	$7.88 \cdot 10^{-1}$	$1.40 \cdot 10^{-1}$	$6.95 \cdot 10^{-1}$	$1.13 \cdot 10^{-2}$	$1.60 \cdot 10^{-2}$ $(nmol)$

Table 3: Approximated values of the standard deviation of each kinetic parameter w.r.t. each of the initial conditions explored using Equation 10. For the definition of surface coverage standard deviations, the variations in the beta distributions were assumed to be accurate approximations. The experimentally observed values of the void and pulse intensity standard deviations were also used, while loose approximations of the pulse delay and location standard deviations were applied.

Variable	$\sigma(k_1^f)$	$\sigma(k_1^b)$	$\sigma(k_2^f)$	$\sigma(k_2^b)$	$\sigma(k_3^f)$	$\sigma(k_4^b)$	$\tilde{\sigma_I}$
CO^*	$2.48 \cdot 10^{-3}$	$1.46 \cdot 10^{0}$	$3.86 \cdot 10^{-3}$	$2.57 \cdot 10^{-2}$	$2.00 \cdot 10^{-6}$	$2.96 \cdot 10^{-2}$	$6.00 \cdot 10^{-3}$
O_2^*	$1.85 \cdot 10^{-1}$	$1.72 \cdot 10^{-1}$	$2.25 \cdot 10^{-1}$	$5.73 \cdot 10^{-1}$	$2.26 \cdot 10^{-3}$	$2.20 \cdot 10^{-2}$	$6.00 \cdot 10^{-3}$
O^*	$2.10 \cdot 10^{0}$	$7.09 \cdot 10^{-3}$	$7.13 \cdot 10^{-2}$	$2.20 \cdot 10^{-2}$	$6.22 \cdot 10^{-4}$	$3.13 \cdot 10^{-1}$	$7.07 \cdot 10^{-2}$
T^{CO}	$2.34 \cdot 10^{-3}$	$9.40 \cdot 10^{-4}$	$2.73 \cdot 10^{-6}$	$1.36 \cdot 10^{-5}$	$1.67 \cdot 10^{-8}$	$3.03 \cdot 10^{-5}$	$5.00 \cdot 10^{-3}$
$void$	$1.23 \cdot 10^{0}$	$2.76 \cdot 10^{-1}$	$7.27 \cdot 10^{-2}$	$4.43 \cdot 10^{-1}$	$3.46 \cdot 10^{-5}$	$2.23 \cdot 10^{-2}$	$5.00 \cdot 10^{-3}$
loc	$8.63 \cdot 10^{-1}$	$1.04 \cdot 10^{-1}$	$8.50 \cdot 10^{-3}$	$3.00 \cdot 10^{-1}$	$5.71 \cdot 10^{-6}$	$8.17 \cdot 10^{-2}$	$1.00 \cdot 10^{-2}$
I^{CO}	$1.16 \cdot 10^{-2}$	$2.76 \cdot 10^{-2}$	$1.17 \cdot 10^{-5}$	$2.00 \cdot 10^{-4}$	$5.23 \cdot 10^{-7}$	$2.44 \cdot 10^{-4}$	$5.00 \cdot 10^{-3}$
I^{O_2}	$4.99 \cdot 10^{-3}$	$3.26 \cdot 10^{-3}$	$3.75 \cdot 10^{-3}$	$4.41 \cdot 10^{-3}$	$2.98 \cdot 10^{-5}$	$2.44 \cdot 10^{-4}$	$5.00 \cdot 10^{-3}$

3.2 Ensemble-based sampling

The sensitivity-based approach is useful because it does not require a probability distribution and gives insight into the global impact of a given initial condition. However, when a probability distribution around the initial conditions is available or can be assumed, the ensemble-based approach can be utilized. This method does not require an assumption that initial conditions follow normal distributions and enables the simultaneous quantification of uncertainty from multiple initial states. Unfortunately, not all initial states have a clearly defined probability distribution. Nonetheless, it is possible to make reasonable assumptions. We start by analyzing two initial conditions that are expected to be normally distributed (pulse intensities and void fractions) in Section 3.2.1, then move to conditions that do not follow normal distributions (surface coverages) in Section 3.2.2. In Section 3.2.3 we analyze the overall uncertainty from these five initial conditions. The influence of zone position and pulse delays are not considered. Zone position cannot be varied continuously due to the nature of the finite element simulation, and is experimentally well defined. Pulse delays have a relatively small impact based on the sensitivity analysis, and their probability distribution is difficult to define since the uncertainty arises from a combination of random noise in the timing and possibly systematic errors arising from discrepancies between the diffusion model and the real system.

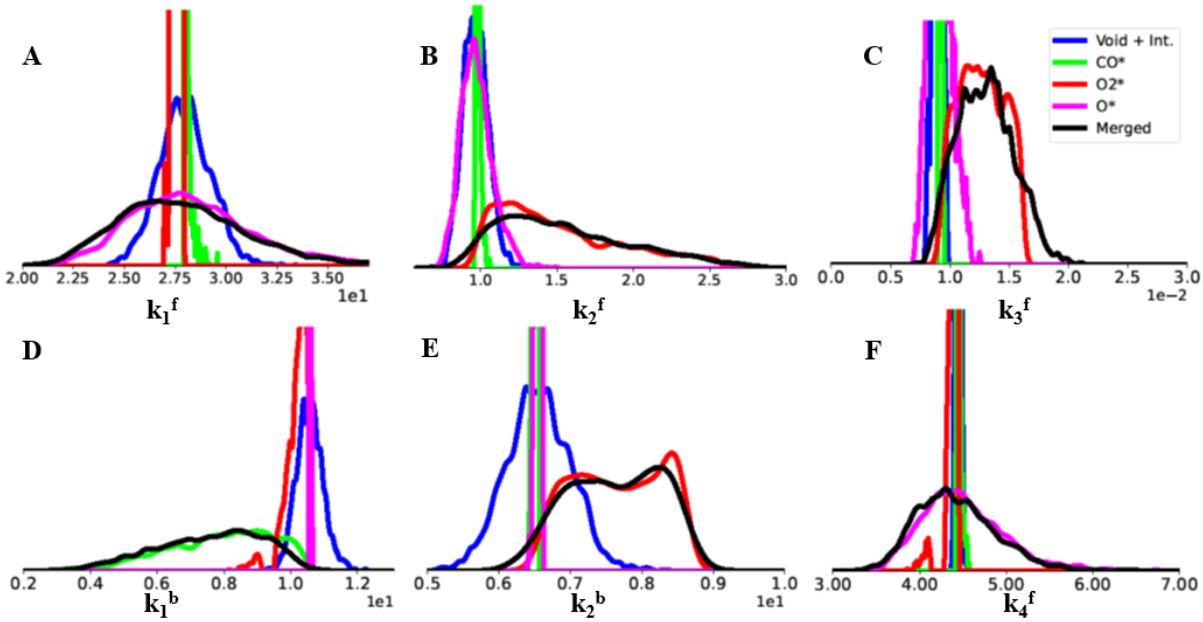

Figure 4: The density plots for each of the kinetic parameters (a-f) using each of the initial conditions ensembles (pulse intensity and void (blue), surface coverages of carbon monoxide (green), molecular oxygen (red), atomic oxygen (pink) and the merged values of a-e (black). Probability densities are plotted using kernel density estimation with specific bandwidths provided in the supplementary information (Section 11).

3.2.1 Normally distributed initial conditions: Pulse intensity and void fraction

The pulse intensities and void fraction are expected to follow normal distributions since the uncertainty comes from random fluctuations and the parameter values are far from physical boundaries. The standard deviations of pulse intensities are expected to be 0.05 nmol (see supplementary information), while the standard deviation of the void fraction is 0.005 [28]. To propagate the uncertainty, 2000 random samples of the probability distributions were generated and the associated parameters refitted.

The distribution of refitted parameters for pulse intensity and void fraction uncertainty propagation are presented in Figure 4 as solid blue lines. These probability distributions follow an approximately Gaussian distribution around their mean values. IQRs can be determined using the percentiles of these distributions and are provided in Table 4. One advantage of normally distributed initial conditions is that the resulting ensembles can be used to construct a statistically rigorous covariance matrix by using Equation 15. The covariance matrix can then be normalized to yield a correlation matrix, which is visualized and compared to the correlation matrix due to experimental noise in Fig. 5 for the uncertainty due to pulse intensities and void fraction.

The experimental noise uncertainty experiences a mixture of highly negative (large, red circles) and positive correlations (large, blue circles) between kinetic parameters, with some parameters experiencing limited correlation (small, faint red circles). The pulse intensity and void ensemble uncertainty was largely positively correlated, except for kinetic parameter k_3^f, which shows little to no correlation with other parameters. The correlation matrix reveals that there are

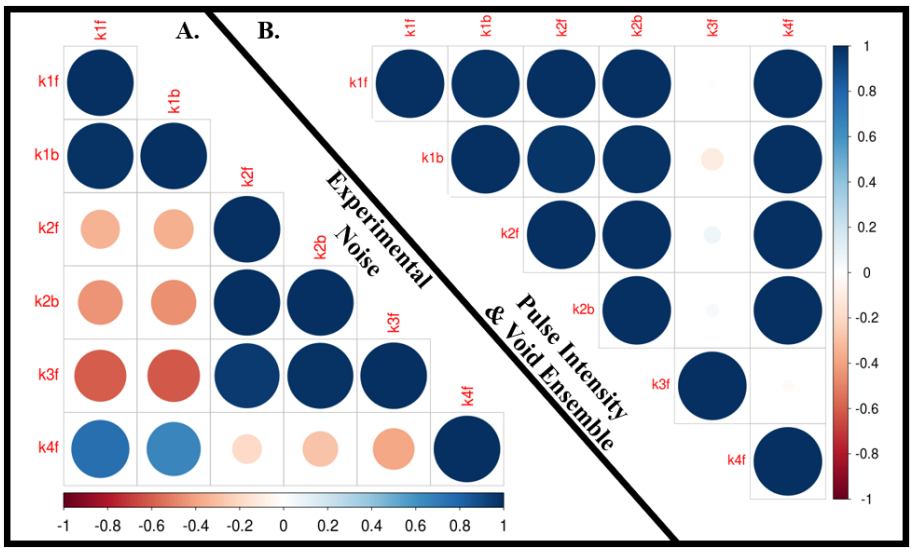

Figure 5: The correlation matrices for the experimental noise uncertainty (a) and the pulse intensity and void ensemble uncertainty (b).

significant correlations between the errors of different parameters, suggesting that uncertainty estimates based on the assumption of independent parameters will tend to overestimate the error.

3.2.2 Beta distributed initial conditions: Surface coverages

While the pulse intensity and void fraction errors are expected to follow normal distributions with known standard deviations, this is not the case for all initial conditions. In particular, surface coverages near zero cannot follow a normal distribution since they are bounded to be positive and less than one, and the variance of surface coverages are typically unknown. However, several surface coverages were found to be highly impactful based on the sensitivity analysis (Tables 2-3), suggesting that the uncertainty in these initial conditions cannot be neglected. To better understand the potential impact these initial states have on the parameters, we make pragmatic assumptions about the initial distribution. The beta distribution (Equations 13 and 14) is used to define the initial coverage of each species. The variances are unknown, but some insight is provided by the objective function values shown in Figure 3. The objective function is relatively flat for the O* coverage, so a conservative standard deviation of $\sim$0.07 ML ($\sigma^2 = 0.005$) is selected. In the case of CO* and O_2* coverages the objective function rises sharply for coverages larger than $\sim$0.02 ML, so a strongly skewed distribution is used to limit coverages to mostly be below this threshold. The resulting distributions are presented in Figure 6, with the atomic oxygen distribution (shape factors of α and β both equal to 50) approximately following a normal distribution and carbon monoxide and molecular oxygen (shape factors of α and β equal to 1.5 and 200, respectively) being skewed heavily toward the 0 boundary. Following the definition of each distribution, initial surface coverages were drawn as samples from the distribution and the kinetic parameters were independently refitted to generate a parameter ensemble. In Figure 4) the green, red and pink lines represent the carbon monoxide, molecular oxygen and atomic oxygen coverage ensembles, respectively.

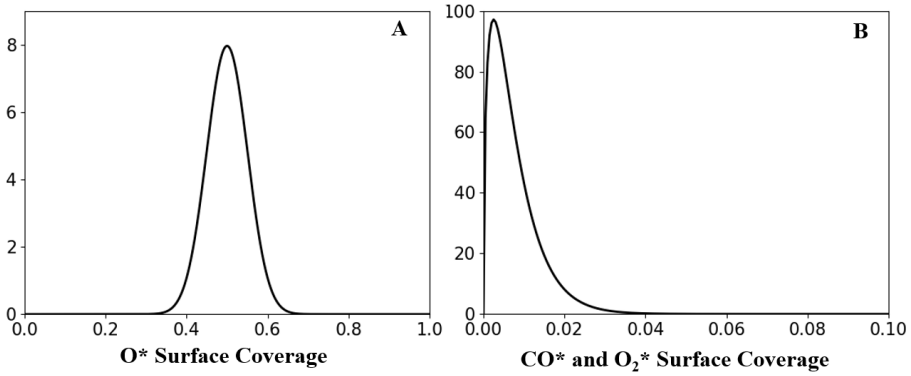

Figure 6: The beta distribution of surface coverages used to propagate uncertainty to the kinetic parameters. The shape parameters for the atomic oxygen coverage (a) are both equal to 50 ($\mu = 0.5$, $\sigma^2 = 5.0 \cdot 10^{-3}$), while their values for carbon monoxide and molecular oxygen (b) are $\alpha = 1.5$ and $\beta = 200$ ($\mu = 7.4 \cdot 10^{-3}$, $\sigma^2 = 3.6 \cdot 10^{-5}$).

First, the uncertainty in carbon monoxide coverage was propagated to the model parameters. Many of the distributions were found to have narrow ranges, especially when compared to those found in the pulse intensity and void ensemble analysis (Figure 4). For example, the values of the parameter k_1^f have an interquartile range (IQR) of $3.00 \cdot 10^{-2}$ for the carbon monoxide surface variation, while it is $1.66 \cdot 10^{0}$ for the pulse intensity and void ensemble. k_1^b is the only parameter to have a significantly wider distribution for the carbon monoxide surface ensemble than the void and pulse intensity ensemble, with an IQR of $2.41 \cdot 10^{0}$, which is consistent with k_1^b being the parameter with the highest relative sensitivity to carbon monoxide coverage. The parameter distributions are also highly skewed, unlike those found in the void and pulse intensity distribution, which follow a generally normal distribution. This can be directly explained by the shape of the initial state distribution (Figure 6). Most parameters are skewed with small variances, similar to the shape of the initial distribution, which indicates a linear response to variations in the CO* coverage. The notable exception is k_1^b, which has a much broader distribution than the CO* distribution. This indicates a that k_1^b is highly non-linear in the CO* coverage, which is not surprising since k_1^b controls CO* desorption. With these non-linear characteristics, the linearity assumption made in the sensitivity analysis may lead to a significant underestimation of the uncertainty associated with this parameter.

Next, the molecular oxygen coverage probability distribution was propagated through the ensemble approach. Similar to the carbon monoxide propagation, some kinetic parameter distributions were found to be narrower or comparable to the void and pulse intensity ensemble. These parameters include k_1^f, k_1^b and k_4^f, which were found to be relatively insensitive to molecular oxygen coverage (Table 2). The other parameters related to oxygen adsorption and dissociation were found to vary significantly based on the molecular oxygen coverage. For example, the IQR of the molecular oxygen ensemble for k_2^f is $5.90 \cdot 10^{-1}$ as compared to $1.13 \cdot 10^{-1}$ for the void and pulse intensity ensemble. Again, the skewed nature of the initial state probability distribution is observed in the kinetic parameter histogram, and strong non-linearities are apparent from the difference in the shape of the distributions, particularly for k_2^b and k_3^f. Notably, the non-linearities also lead to a shift in the mean of the distributions, suggesting that initial state uncertainties can affect the expectation values of kinetic parameters.

Last, the atomic oxygen coverage distribution was propagated through the ensemble approach. Of the kinetic parameter histograms, k_1^b, k_2^b and k_2^f were found to have a narrower or comparable range of values compared to the void and pulse intensity ensemble. Based on the sensitivity analysis, the atomic oxygen coverage was expected to have a small influence compared to the other initial coverages. However, the results of the ensemble approach show that the resulting k_1^f distribution has a higher variance than for any other initial conditions, including the void fraction. This observation illustrates that the sensitivity analysis does not account for the overall variance in the initial conditions. The variance of the O* coverage distribution was determined to be larger than CO* or O_2* based on the objective function values from the continuous parameter variation analysis (Fig. 3). For atomic oxygen, the variance of the coverage distribution was selected to be $5.0 \cdot 10^{-3}$ ML, which is far larger than the variance of carbon monoxide and molecular oxygen coverages ($3.6 \cdot 10^{-5}$ ML). This larger variance, rather than the local sensitivity, then results in a larger impact of the O* coverage on the k_1^f parameter. This results of the ensemble analysis reveal the complex interplay between initial condition uncertainty, non-linearities in the model, and the ultimate uncertainty on kinetic parameters.

Table 4: The interquartile range (IQR) for the parameters in the kinetic model found through ensemble based sampling of different sets of individual initial conditions, as well as the total ensemble (TE), the signal noise (SN) and merged covariance calculation (AE & SN calculated with Equation 16).

	Source	P_i & v	θ_{CO}	θ_{O_2}	θ_O	TE	SN	TE & SN
k_1^f	Median	$2.79 \cdot 10^{1}$	$2.80 \cdot 10^{1}$	$2.76 \cdot 10^{1}$	$2.80 \cdot 10^{1}$	$2.76 \cdot 10^{1}$	$2.80 \cdot 10^{1}$	$2.80 \cdot 10^{1}$
	IQR	$1.66 \cdot 10^{0}$	$3.00 \cdot 10^{-2}$	$3.47 \cdot 10^{-1}$	$3.96 \cdot 10^{0}$	$4.23 \cdot 10^{0}$	$3.77 \cdot 10^{-1}$	$4.39 \cdot 10^{0}$
k_1^b	Median	$1.06 \cdot 10^{1}$	$8.10 \cdot 10^{0}$	$1.02 \cdot 10^{1}$	$1.06 \cdot 10^{1}$	$7.75 \cdot 10^{0}$	$1.06 \cdot 10^{1}$	$1.06 \cdot 10^{1}$
	IQR	$5.16 \cdot 10^{-1}$	$2.41 \cdot 10^{0}$	$3.87 \cdot 10^{-1}$	$1.47 \cdot 10^{-2}$	$2.36 \cdot 10^{0}$	$1.38 \cdot 10^{-1}$	$2.15 \cdot 10^{0}$
k_2^f	Median	$9.65 \cdot 10^{-1}$	$9.72 \cdot 10^{-1}$	$1.39 \cdot 10^{0}$	$9.64 \cdot 10^{-1}$	$1.46 \cdot 10^{0}$	$9.63 \cdot 10^{-1}$	$9.63 \cdot 10^{-1}$
	IQR	$1.13 \cdot 10^{-1}$	$1.17 \cdot 10^{-2}$	$5.90 \cdot 10^{-1}$	$1.34 \cdot 10^{-1}$	$6.40 \cdot 10^{-1}$	$9.03 \cdot 10^{-3}$	$6.65 \cdot 10^{-1}$
k_2^b	Median	$6.55 \cdot 10^{0}$	$6.51 \cdot 10^{0}$	$7.61 \cdot 10^{0}$	$6.56 \cdot 10^{0}$	$7.60 \cdot 10^{0}$	$6.56 \cdot 10^{0}$	$6.56 \cdot 10^{0}$
	IQR	$2.86 \cdot 10^{-1}$	$4.00 \cdot 10^{-2}$	$1.14 \cdot 10^{0}$	$4.13 \cdot 10^{-2}$	$2.36 \cdot 10^{0}$	$1.01 \cdot 10^{-1}$	$2.10 \cdot 10^{0}$
k_3^f	Median	$9.05 \cdot 10^{-3}$	$9.07 \cdot 10^{-3}$	$1.27 \cdot 10^{-2}$	$9.05 \cdot 10^{-3}$	$1.31 \cdot 10^{-2}$	$9.05 \cdot 10^{-3}$	$9.05 \cdot 10^{-3}$
	IQR	$3.97 \cdot 10^{-4}$	$6.66 \cdot 10^{-5}$	$3.33 \cdot 10^{-3}$	$1.18 \cdot 10^{-3}$	$3.66 \cdot 10^{-3}$	$1.90 \cdot 10^{-4}$	$2.22 \cdot 10^{-1}$
k_4^b	Median	$4.45 \cdot 10^{0}$	$4.43 \cdot 10^{0}$	$4.40 \cdot 10^{0}$	$4.44 \cdot 10^{0}$	$4.36 \cdot 10^{0}$	$4.45 \cdot 10^{0}$	$4.45 \cdot 10^{0}$
	IQR	$3.15 \cdot 10^{-2}$	$1.40 \cdot 10^{-2}$	$5.50 \cdot 10^{-2}$	$6.13 \cdot 10^{-1}$	$6.03 \cdot 10^{-1}$	$3.43 \cdot 10^{-2}$	$6.26 \cdot 10^{-1}$

3.2.3 Merged ensemble analysis

The ensemble approach provides a convenient route for simultaneously propagating the uncertainty of all initial conditions to the kinetic parameters. For the merged analysis, each run involves randomly sampling from all initial conditions based on their probability distributions and refitting the kinetic parameters based on the output. The resulting distributions of kinetic parameters are presented in Figure 4 as black lines. The variance of the resulting merged parameter ensembles is highly correlated with the broadest individual ensembles. This is consistent with the fact that the total ensemble median and IQRs in Table 16 are approximately equal to the median and IQR based on the initial state with the largest IQR, and suggests that there is typically a single initial state that dominates the uncertainty of a given parameter. However, the initial state that is most important varies between different parameters, meaning multiple initial state uncertainties need to be considered. This makes the merged ensemble approach powerful, since it allows for accounting for the uncertainty of all of the most impactful initial states in a single run.

4 Discussion

The ensemble approach is the most direct method of analysis and has the most flexible assumptions. With the approach, the influence of complex initial state distributions (i.e. non-Gaussian) on kinetic parameters can be observed, multiple initial state uncertainties can be propagated simultaneously, and covariance information is provided. However, a challenge with the ensemble approach is the need to specify an initial distribution, and the computational resources necessary to perform the full ensemble of simulations. The sensitivity analysis is an alternative approach that provides

insight into the local sensitivity at a reduced computational cost. This method only requires a single additional calculation per initial state of interest (as opposed to the thousands of calculations necessary for the ensemble approach). However, it is restricted to the assumptions that the uncertainty in the initial states follows a normal distribution, that the uncertainties on parameters from different initial conditions are independent, and that the objective function is linear in the parameters over the range of initial conditions. When the sensitivity approach is applied to the problem in Section 3.2.1, moderate agreement between the IQR from the sensitivity analysis and the ensemble approach are observed (see Table 5). Although exact matches are not obtained, the values fall within the same order of magnitude in most cases. Cases where the sensitivity approach over-estimates the uncertainty can be explained by correlations in the parameters with respect to initial conditions (Fig. 5), while the ensemble estimates are higher due to nonlinear dependencies between initial conditions and parameters.

Table 5: Values of the IQR for the pulse intensity and void uncertainties calculated through the sensitivity (using Equation 11) and ensemble approaches (Section 3.2.1).

Method	k_1^f	k_1^b	k_2^f	k_2^b	k_3^f	k_4^b
Sensitivity	$1.65\cdot 10^{0}$	$5.25\cdot 10^{-1}$	$1.10\cdot 10^{-1}$	$5.96\cdot 10^{-1}$	$4.02\cdot 10^{-4}$	$3.18\cdot 10^{-2}$
Ensemble	$1.66\cdot 10^{0}$	$5.16\cdot 10^{-1}$	$1.13\cdot 10^{-1}$	$2.86\cdot 10^{-1}$	$3.97\cdot 10^{-4}$	$3.15\cdot 10^{-2}$

Of the initial conditions explored, the pulse delays and intensities appeared to have the least impact on the kinetic parameter values. Although increasing the uncertainty in these initial states would increase their impact, they are relatively well-defined experimentally. The void fraction was found to have a much higher sensitivity (Table 2) than the pulse delay and intensity. Like the delays and intensities, the void fraction is a well-defined quantity with a normal distribution and a small standard deviation, so propagating the uncertainty is easily performed and cheap (if the sensitivity approach is used) [28]. The catalyst location was found to have a sensitivity in the range of pulse intensities and delays, but the precision of the catalyst location is dependent on the preparation procedures. Assuming the bed is prepared such that the location is well defined, the location uncertainty will not significantly impact the model parameters.

The most important initial conditions to consider are the surface coverages, which were found to generally have the highest sensitivities of the initial conditions. Furthermore, these are the most challenging initial conditions to define, leading to wide distributions and potentially complex shapes. The global sensitivity analysis can provide insight into the uncertainty on the initial surface coverages by evaluating the objective function value with respect to each coverage. If the objective function is sensitive to the coverage it is reasonable to assume that the relevant surface coverages are those near the minimum of the objective function. However, as the number of adsorbed species increases, it is likely that the objective function will be insensitive to more initial coverages. Moreover, the computational cost of propagating uncertainty will also increase with the number of adsorbed species and the variance of their initial coverages, since the fitting procedure converges more slowly in higher dimensions and when the initial guess is farther from the solution. For

this reason, careful experimental characterization of the initial state of the catalyst surface, or operando spectroscopic techniques that directly measure the concentrations of surface species, may be required to reduce the uncertainty of parameters extracted from TAP experiments on complex reaction networks.

A common goal in surface science and catalysis is determining free energies of activation for elementary steps. This is commonly achieved using DFT, which has a standard deviation of around 0.2 eV [4, 3, 31]. To compare the uncertainty of TAP-derived parameters to DFT energies, we convert the rate constants to free energies of activation ($\Delta G^{\ddagger}$) via the Eyring equation

$$k = \frac{k_b T}{h} \exp\left(-\frac{\Delta G^{\ddagger}}{RT}\right) \tag{17}$$

where k_b is the Boltzmann's constant, T is temperature, h is Planck's constant, $\Delta G^{\ddagger}$ is the free energy of activation and R is the ideal gas constant [32]. The lower and upper quartiles of the activation energies corresponding to each rate constant are presented in Table 4. The IQR due to initial state uncertainty is generally $<$0.02 eV, or an order of magnitude lower than DFT. The IQR from experimental noise is also generally small (IQR of $<$0.002). An exception to this trend is parameter $\delta G_3^{f\ddagger}$, where the IQR includes an imaginary number (due to the lower bound of the IQR for kinetic parameter k_3^f falling in the negative domain). This arises from the combination of a Gaussian (from signal noise) and non-Gaussian distribution (from the ensemble analysis), where the non-Gaussian distribution skews heavily in a positive direction. When the two covariance matrices are merged (using Equation 16), it is assumed that they have the same mean value. This assumption works for the other kinetic parameters, but fails for $G_3^{f\ddagger}$, which has a much broader IQR relative to the assumed mean value of the parameter. Nonetheless, the low uncertainty values for each separate analysis (0.01 - 0.001 eV) suggest that the error on this parameter is also small.

The low uncertainties in this study are encouraging for the use of TAP as a route to extracting kinetic parameters, but there are several important caveats. First, this case study is based on a relatively simple and well-studied reaction and catalyst (carbon monoxide oxidation over platinum). The results may not generalize to more complex reaction systems, indicating that uncertainty quantification studies should be performed whenever kinetic parameters are extracted from TAP data. Moreover, without good estimates of the uncertainty on initial conditions, it is impossible to get good estimates of the uncertainty on the kinetic parameters, therefore it is important to continue to develop numerical and experimental techniques to improve the precision of initial conditions and flux data obtained from TAP experiments. Finally, there is the challenging but important issue of structural uncertainty arising from the assumed mechanism and active site(s) used in the kinetic model. This uncertainty is difficult to quantify, but likely has a more significant influence than initial state or experimental noise uncertainty. However, the same issue exists in DFT calculations, but manifests differently as the assumptions around the atomic structure of the active site. The fundamental differences in the sources of structural uncertainty suggest that TAP (or other transient kinetic measurements) and DFT should be viewed as complementary techniques, where agreement between the two is strong evidence supporting the hypothesized mechanism and active site structure.

Table 6: The IQR of the free energies of activation for each parameter calculated with the Eyring equation for each of the ensembles calculated in Section 3. These distributions fall well below those typically found in DFT and point toward the potential utility of TAP experimental analysis. The free energy IQR for AE & SN in parameter k_3^f was found to have an imaginary value (due to the left bound of the IQR being negative), and is therefore labeled with a dash.

Uncertainty Source	$G_1^{f\ddagger}$	$G_1^{b\ddagger}$	$G_2^{f\ddagger}$	$G_2^{b\ddagger}$	$G_3^{f\ddagger}$	$G_4^{b\ddagger}$
P_i & v	$2.93\cdot 10^{-3}$	$2.41\cdot 10^{-3}$	$5.79\cdot 10^{-3}$	$2.21\cdot 10^{-3}$	$2.17\cdot 10^{-3}$	$3.50\cdot 10^{-4}$
θ_{CO}	$5.30\cdot 10^{-5}$	$1.50\cdot 10^{-2}$	$5.93\cdot 10^{-4}$	$3.03\cdot 10^{-4}$	$3.62\cdot 10^{-4}$	$1.56\cdot 10^{-4}$
θ_{O_2}	$6.21\cdot 10^{-4}$	$1.86\cdot 10^{-3}$	$2.02\cdot 10^{-2}$	$7.37\cdot 10^{-3}$	$1.28\cdot 10^{-2}$	$6.18\cdot 10^{-4}$
θ_O	$6.98\cdot 10^{-3}$	$6.87\cdot 10^{-5}$	$6.89\cdot 10^{-3}$	$3.11\cdot 10^{-4}$	$6.41\cdot 10^{-3}$	$6.78\cdot 10^{-3}$
All Ensemble (AE)	$7.54\cdot 10^{-3}$	$1.54\cdot 10^{-2}$	$2.14\cdot 10^{-2}$	$1.54\cdot 10^{-2}$	$1.39\cdot 10^{-2}$	$6.80\cdot 10^{-3}$
Signal Noise (SN)	$6.59\cdot 10^{-4}$	$6.36\cdot 10^{-4}$	$4.60\cdot 10^{-4}$	$7.54\cdot 10^{-4}$	$1.03\cdot 10^{-3}$	$3.78\cdot 10^{-4}$
AE & SN	$7.75\cdot 10^{-3}$	$1.00\cdot 10^{-2}$	$3.56\cdot 10^{-2}$	$1.59\cdot 10^{-2}$	–	$6.96\cdot 10^{-3}$

5 Conclusion

In this article, we introduced two methods for exploring the impact of uncertainty on TAP initial states on the rate constants obtained from PDE-constrained optimization using TAP experimental data. First, a sensitivity-based approach was introduced, which involves changing the initial states independently and observing shifts in the parameter values. Second, an ensemble-based approach was developed, which involves drawing random samples from probability distributions defined around the initial states. We apply these techniques to a case study of carbon monoxide oxidation on platinum, and compare the initial state uncertainty to experimental noise uncertainty.

The results indicate that the two uncertainty quantification techniques are complementary. The sensitivity analysis provides computationally efficient estimates of which initial conditions are most important, and a global sensitivity analysis can be used to identify the ranges of initial conditions where the objective function is near its minimum. The ensemble approach enables a more comprehensive evaluation of the uncertainty, including the covariance between parameters and the impact of initial conditions that do not follow normal distributions. In the case study presented, the results of both approaches were qualitatively similar and indicate that the uncertainty in initial surface coverage is likely the dominant source of initial state uncertainty.

A comparison of uncertainty from initial states and experimental noise indicates that in this case study the initial state uncertainties are dominant. However, this conclusion may not be general to more complex reactions, and the tools presented provide a practical route to evaluating both experimental noise and initial state uncertainty in other studies. Moreover, in this case study the uncertainty in activation free energies from both initial states and experimental noise ($\lesssim$0.02 eV) is more around one order of magnitude lower than that of typical GGA DFT calculations ($\sim$ 0.2 eV). This suggests that rate constants derived from TAP experiments are a promising complement to DFT calculations, although structural uncertainty remains a challenge for both techniques.

Acknowledgements

Support for this work was provided by the U.S. Department of Energy (USDOE), Office of Energy Efficiency and Renewable Energy (EERE), Advanced Manufacturing Office Next Generation R&D Projects under contract no. DE-AC07-05ID14517.

This research made use of Idaho National Laboratory computing resources which are supported by the Office of Nuclear Energy of the U.S. Department of Energy and the Nuclear Science User Facilities under Contract No. DE-AC07-05ID14517.

Conflict of Interest

The authors declare no competing financial interest.

References

[1] N. Mizuno and M. Misono, "Heterogeneous catalysis," *Chemical Reviews*, vol. 98, no. 1, pp. 199–218, 1998.

[2] S. Matera, W. F. Schneider, A. Heyden, and A. Savara, "Progress in accurate chemical kinetic modeling, simulations, and parameter estimation for heterogeneous catalysis," *ACS Catalysis*, vol. 9, no. 8, pp. 6624–6647, 2019.

[3] A. J. Medford, M. R. Kunz, S. M. Ewing, T. Borders, and R. Fushimi, "Extracting knowledge from data through catalysis informatics," *ACS Catalysis*, vol. 8, no. 8, pp. 7403–7429, 2018.

[4] J. Wellendorff, T. L. Silbaugh, D. Garcia-Pintos, J. K. Nørskov, T. Bligaard, F. Studt, and C. T. Campbell, "A benchmark database for adsorption bond energies to transition metal surfaces and comparison to selected dft functionals," *Surface Science*, vol. 640, pp. 36–44, 2015.

[5] J. Feng, J. L. Lansford, M. A. Katsoulakis, and D. G. Vlachos, "Explainable and trustworthy artificial intelligence for correctable modeling in chemical sciences," *Science advances*, vol. 6, no. 42, p. eabc3204, 2020.

[6] J. T. Gleaves, G. S. Yablonskii, P. Phanawadee, and Y. Schuurman, "Tap-2: An interrogative kinetics approach," *Applied Catalysis A: General*, vol. 160, no. 1, pp. 55–88, 1997.

[7] J. T. Gleaves, G. Yablonsky, X. Zheng, R. Fushimi, and P. L. Mills, "Temporal analysis of products (tap)—recent advances in technology for kinetic analysis of multi-component catalysts," *Journal of Molecular Catalysis A: Chemical*, vol. 315, no. 2, pp. 108–134, 2010.

[8] K. Morgan, N. Maguire, R. Fushimi, J. Gleaves, A. Goguet, M. Harold, E. Kondratenko, U. Menon, Y. Schuurman, and G. Yablonsky, "Forty years of temporal analysis of products," *Catalysis Science & Technology*, vol. 7, no. 12, pp. 2416–2439, 2017.

[9] J. E. Sutton, W. Guo, M. A. Katsoulakis, and D. G. Vlachos, "Effects of correlated parameters and uncertainty in electronic-structure-based chemical kinetic modelling," *Nature chemistry*, vol. 8, no. 4, pp. 331–337, 2016.

[10] A. J. Medford, J. Wellendorff, A. Vojvodic, F. Studt, F. Abild-Pedersen, K. W. Jacobsen, T. Bligaard, and J. K. Nørskov, "Assessing the reliability of calculated catalytic ammonia synthesis rates," *Science*, vol. 345, no. 6193, pp. 197–200, 2014.

[11] E. Walker, S. C. Ammal, G. A. Terejanu, and A. Heyden, "Uncertainty quantification framework applied to the water–gas shift reaction over pt-based catalysts," *The Journal of Physical Chemistry C*, vol. 120, no. 19, pp. 10328–10339, 2016.

[12] C. Waldron, A. Pankajakshan, M. Quaglio, E. Cao, F. Galvanin, and A. Gavriilidis, "Closed-loop model-based design of experiments for kinetic model discrimination and parameter estimation: Benzoic acid esterification on a heterogeneous catalyst," *Industrial & Engineering Chemistry Research*, vol. 58, no. 49, pp. 22165–22177, 2019.

[13] C. Waldron, A. Pankajakshan, M. Quaglio, E. Cao, F. Galvanin, and A. Gavriilidis, "Model-based design of transient flow experiments for the identification of kinetic parameters," *Reaction Chemistry & Engineering*, vol. 5, no. 1, pp. 112–123, 2020.

[14] Z. Ulissi, V. Prasad, and D. Vlachos, "Effect of multiscale model uncertainty on identification of optimal catalyst properties," *Journal of catalysis*, vol. 281, no. 2, pp. 339–344, 2011.

[15] P. Plechac and D. G. Vlachos, "Final technical report: Mathematical foundations for uncertainty quantification in materials design," tech. rep., Univ. of Delaware, Newark, DE (United States), 2018.

[16] J. E. Sutton and D. G. Vlachos, "Effect of errors in linear scaling relations and brønsted–evans–polanyi relations on activity and selectivity maps," *Journal of Catalysis*, vol. 338, pp. 273–283, 2016.

[17] J. Feng, J. Lansford, A. Mironenko, D. B. Pourkargar, D. G. Vlachos, and M. A. Katsoulakis, "Non-parametric correlative uncertainty quantification and sensitivity analysis: Application to a langmuir bimolecular adsorption model," *AIP Advances*, vol. 8, no. 3, p. 035021, 2018.

[18] M. Cohen and D. G. Vlachos, "Chemical kinetics bayesian inference toolbox (ckbit)," *Computer Physics Communications*, vol. 265, p. 107989, 2021.

[19] W. Chen, M. Cohen, K. Yu, H.-L. Wang, W. Zheng, and D. G. Vlachos, "Experimental data-driven reaction network identification and uncertainty quantification of co2-assisted ethane dehydrogenation over ga2o3/al2o3," *Chemical Engineering Science*, vol. 237, p. 116534, 2021.

[20] A. Savara and E. A. Walker, "Chekipeuq intro 1: Bayesian parameter estimation considering uncertainty or error from both experiments and theory," *ChemCatChem*.

[21] E. Redekop, D. Constales, G. Yablonsky, G. Marin, and U. Olsbye, "Assessing the interplay of spatial and temporal uncertainties in the catalyst state during temporal analysis of products (tap) kinetic experiments,"

[22] D. Constales, S. Shekhtman, G. Yablonsky, G. Marin, and J. Gleaves, "Multi-zone tap-reactors theory and application iv. ideal and non-ideal boundary conditions," *Chemical Engineering Science*, vol. 61, no. 6, pp. 1878–1891, 2006.

[23] A. Yonge, M. R. Kunz, R. Batchu, Z. Fang, T. Issac, R. Fushimi, and A. J. Medford, "Tapsolver: A python package for the simulation and analysis of tap reactor experiments," *Chemical Engineering Journal*, p. 129377, 2021.

[24] R. Roelant, D. Constales, G. S. Yablonsky, R. Van Keer, M. A. Rude, and G. B. Marin, "Noise in temporal analysis of products (tap) pulse responses," *Catalysis today*, vol. 121, no. 3-4, pp. 269–281, 2007.

[25] R. Roelant, *Mathematical determination of reaction networks from transient kinetic experiments*. PhD thesis, Ghent University, 2011.

[26] M. R. Kunz, A. Yonge, Z. Fang, R. Batchu, A. J. Medford, D. Constales, G. Yablonsky, and R. Fushimi, "Data driven reaction mechanism estimation via transient kinetics and machine learning," *Chemical Engineering Journal*, p. 129610, 2021.

[27] H. H. Ku *et al.*, "Notes on the use of propagation of error formulas," *Journal of Research of the National Bureau of Standards*, vol. 70, no. 4, pp. 263–273, 1966.

[28] G. Mallol, J. Amorós, M. Orts, and D. Llorens, "Densification of monomodal quartz particle beds by tapping," *Chemical Engineering Science*, vol. 63, no. 22, pp. 5447–5456, 2008.

[29] P. Virtanen, R. Gommers, T. E. Oliphant, M. Haberland, T. Reddy, D. Cournapeau, E. Burovski, P. Peterson, W. Weckesser, J. Bright, *et al.*, "Scipy 1.0: fundamental algorithms for scientific computing in python," *Nature methods*, vol. 17, no. 3, pp. 261–272, 2020.

[30] J. Nunez-Iglesias, S. Van Der Walt, and H. Dashnow, *Elegant SciPy: The art of scientific python*. " O'Reilly Media, Inc.", 2017.

[31] C. Reece and R. J. Madix, "Moving from fundamental knowledge of kinetics and mechanisms on surfaces to prediction of catalyst performance in reactors," *ACS Catalysis*, vol. 11, no. 5, pp. 3048–3066, 2021.

[32] J. C. Polanyi, "Concepts in reaction dynamics," *Accounts of Chemical Research*, vol. 5, no. 5, pp. 161–168, 1972.